Available online at www.sciencedirect.com

SCIENCE DIRECT®

Earth and Planetary Science Letters 228 (2004) 65–84

EPSL

www.elsevier.com/locate/epsl

Melting and dissolution of subducting crust at high pressures: the key role of white mica

Max W. Schmidt[a,*], Daniel Vielzeuf[b], Estelle Auzanneau[b]

[a] *Institute for Mineralogy and Petrology, ETH, 8092 Zürich, Switzerland*
[b] *Laboratoire Magmas et Volcans, CNRS and Université Blaise Pascal, 5 rue Kessler, 63038 Clermont-Ferrand, France*

Received 24 April 2004; received in revised form 7 September 2004; accepted 7 September 2004
Editor: V. Courtillot

Abstract

Conditions of melting in the crust are generally controlled by the availability of aqueous fluid and, in the absence of fluid, by the stability of hydroxylated minerals. To depths of 80–90 km, melting is controlled by amphibole and biotite. At greater depths, both phases are unstable in crustal compositions. Simultaneous experiments on a mid-ocean ridge basalt (MORB), a greywacke, and a pelite with excess H_2O of 0.4–1.4 wt.% demonstrate that, at >100 km depth (≥3.5 GPa), all three bulk compositions are composed of garnet+clinopyroxene+phengite+coesite±kyanite±rutile, phengitic white mica being the only hydrous mineral present at near-melting temperatures. At 4 GPa, melting reactions, temperatures, and initial melt compositions are thus similar in the entire subducted crust. Fluid-saturated initial melting takes place near 850 °C and melt productivities are proportional to phengite contents. All three bulk compositions produce initially slightly peraluminous potassic Si-rich granites with K:Na molar ratios of 1.4–2.0 and containing 8–13 wt.% H_2O. The relatively low Na-contents of these melts result from clinopyroxene/melt partitioning coefficients ($D^{cpx/melt}$) of 2.2–4.0 at near solidus temperatures.

At higher pressures (≥6.5 GPa), we infer that classical melting does not take place. Instead, the bulk H_2O-contents (1.5–2.1 wt.%) in the starting materials, although low, are apparently sufficient to dissolve phengite entirely near 1050 °C. This suggests that pressure conditions beyond the singular endpoint (or second critical point) which terminates the wet solidus as defined by Ricci in 1951 [J.E. Ricci, The phase rule and heterogeneous equilibrium, Dover Publications, Inc. New York (1951) 505 p.] were reached for all three bulk compositions. Extraction of these "supercritical" solute-rich (but Na-poor) melts, which contain about 30–40% H_2O, or extraction of the potassic granite melts at lower pressure leave an anhydrous garnet+clinopyroxene±coesite±kyanite±rutile residue. Our results suggest that, except for extremely cold subduction zones, the subducting crust will lose all its potassium (and most of B, Be, Rb, and Ba, and other phengite-hosted trace elements) through leaching or melting during its descent to 300 km. The potassium-rich silica-saturated liquids will immediately react with the peridotite when entering the mantle wedge thus creating source regions for ultrapotassic magmas.

* Corresponding author. Tel.: +41 1 632 7988; fax: +41 1 632 1088.
E-mail address: max.schmidt@erdw.ethz.ch (M.W. Schmidt).

0012-821X/$ - see front matter © 2004 Elsevier B.V. All rights reserved.
doi:10.1016/j.epsl.2004.09.020

1. Introduction

One of the driving forces of arc magmatism is the alteration of the mantle wedge by fluids or melts derived from the subducting crust [2,3]. Hydroxylated minerals and, to a minor extent, carbonates play a key role in this process as they either liberate fluid through a sequence of subsolidus dehydration reactions [4] or participate in melting reactions [5,6]. Stabilities and amounts of hydroxylated minerals [4,7–9] and carbonates [10,11] have been experimentally established for low and intermediate temperature conditions. However, for warmer slabs, melting in crustal compositions at elevated pressures (i.e., >3 GPa) is poorly understood, and published experimental data on metasedimentary compositions [7,12–14] show large discrepancies (Fig. 1).

In sedimentary and mafic bulk compositions, volumetrically minor fluid-absent melting reactions involving muscovite and zoisite define the minimum temperature for fluid-absent melting at crustal pressures [6]. The volumetrically major fluid-absent melting reactions involve biotite and amphibole, respectively, and have been thoroughly investigated to pressures of 2.5 GPa for biotite [15,16] and amphibole [16,17]. Nevertheless, amphibole, zoisite [4], and biotite [18] become unstable in bulk compositions of the oceanic crust at pressures ≤3 GPa and are no longer available for melting at higher pressures. Previous experimental studies [4,7,12,19] and calculations [20] suggest that phengite (i.e., Si-rich white mica) is the most likely (and only) hydrous subsolidus mineral at near-melting temperatures and pressures greater than 3 GPa. Phengite, which is stable up to 8.5 and 9.5 GPa in metapelites and metabasalts, respectively, is thus potentially involved in melting (and dissolution) reactions in the depth range of 100–300 km. In addition, as phengite is the principal host of several key trace elements in the subduction process (B, Be, Rb, and Cs [21]), its fate is directly linked to the recycling of these elements.

The concept of ‘solidus’ and ‘aqueous fluid’ clearly distinguished from ‘hydrous silicate melt’ becomes invalid at high pressures when the solvus between a low-density aqueous fluid and a dense hydrous silicate melt closes [1,22–24]. Thus, at pressures above the intersection of the classical fluid-saturated solidus with the closure of the fluid–melt solvus (i.e., the singular endpoint defined by Ricci [1], p. 68 ff], termed the “second critical point” by Boettcher and Wyllie [22]), a classical

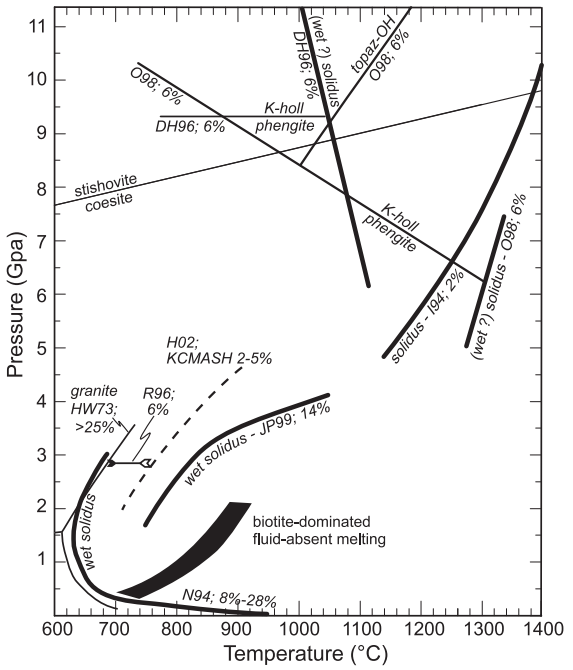

Fig. 1. Pressure–temperature diagram illustrating the contradictory determinations of solidi (bold lines) and phengite→K-hollandite reactions in natural K_2O-rich bulk compositions. The phengite-out in a Na- and Fe-free synthetic system as given by [34] is indicated by the stippled line (H02). The wet solidus to 3 GPa is from Nicholls et al. (N94 [32], and references therein), and directly compared to the wet granite solidus from Huang and Wyllie (thin line below 3.5 GPa, HW73, [31]). The bracket at 2.85 GPa is from Ryabchikov et al. (R96 [33]) on a broadly andesitic composition. The stippled line gives the solidus determined for a simple K_2O–CaO–MgO–Al_2O_3–SiO_2–H_2O system by Hermann (H02 [34]). As expected, the solidus in this FeO- and Na_2O-free system is somewhat higher (approximately 80 °C) than in natural metapelites. The wet solidus from 2 to 4 GPa of Johnson and Plank (JP99 [14]) is inconsistent with the other studies in this pressure range. As can be seen, the high-pressure solidi and the phengite stability limit from Ono (O98 [7]) and Domanik and Holloway (DH96 [12]) are inconsistent as given. Irifune et al. (I94 [13]) studied an average continental crust composition in which FeO was replaced by CoO. In this study, the bulk H_2O content was 2 wt.% and their solidus might correspond to a fluid-absent solidus. The dark band indicates conditions of fluid-absent biotite dominated melting at crustal pressures (after [15,16]). The length of the lines corresponds to the experimental P–T range investigated, the percentage values give experimental H_2O-contents in the starting material.

melting regime ceases to exist. The discontinuous solidus reaction involving an aqueous fluid on the low temperature side and a hydrous melt on the high temperature side is then replaced by a continuous reaction as only one noncrystalline phase may coexist with the solid phases at pressures beyond the singular endpoint of the solidus. With increasing temperature, this liquid (a new critical phase) then spans a chemical continuum between the compositions of aqueous fluid and hydrous melt at lower pressure. Some discrepancies in existing high-pressure "melting" studies may be attributed to the interpretation of the experimental data within a classical melting scheme, at conditions where it is no longer appropriate. The pressures at which classical solidi end are strongly dependant on bulk composition and the few available studies indicate values between 0.97 GPa for the SiO_2–H_2O system [25] and >12 GPa for the MgO–SiO_2–H_2O system [24]. One aim of this study is to define the pressures of the solidus' endpoint in bulk compositions of the oceanic crust, i.e., in MORB, greywacke, and pelite. More generally, we investigate high-pressure mineralogy, melting, and dissolution reactions in these three bulk compositions as relevant for subduction zones.

2. Experimental techniques

2.1. Experimental apparatus

Experiments at pressures at, and above, 4 GPa were performed in a Walker type multianvil module employing 32-mm edge length WC-cubes with 17-mm truncation edge lengths (TEL). The assembly was composed of a 25-mm edge length octahedron, a stabilized zirconia insulation sleeve, a stepped $LaCrO_3$ furnace with a graphite disc and ring between furnace and WC-cubes, and inner MgO liners. In order to avoid perforation of the capsules, an axial mullite thermocouple ceramic with approximately 30% porosity (close to the octahedron porosity of 32%) was employed, together with an *S*-type thermocouple (Pt–$Pt_{90}Rh_{10}$). The central thickened part of the furnace contained two 2.0 mm OD or three 1.6 mm OD gold capsules parallel to the furnace. Before loading, the welded Au-capsules were pressed into one cylinder (3.1 mm in diameter and 3.5 mm long). An experiment with two thermocouples (without capsules) located in the predicted hot and cold spots showed that this setup generates a temperature gradient less than 11 °C (at 1000 °C) across the length of the capsules. Pressure was calibrated against the quartz–coesite [26], $CaGeO_3$ garnet–perovskite [27], and coesite–stishovite [28] transitions at 900 °C. The experiment at 3.5 GPa was performed in an end-loaded 1/2-in. piston cylinder with a salt–graphite–MgO cell and an *S*-type thermocouple.

2.2. Starting materials

The MOR basalt (TMB-7) is composed of a mixture of synthetic glass and $Al(OH)_3$ (Table 1). Previous experience [19] showed that it is very difficult to detect K-bearing phases in MORB with its typically low K_2O content (0.3 wt.%). Thus, the MORB composition TMB-7 corresponds to an average MORB enriched in K_2O (0.9 wt.%), leading to 8 wt.% phengite if all potassium is stored in this mineral. A mixture of oxides, albite, a $KMg_{0.5}Al_{1.83}Si_{3.5}O_{10}$ glass (controlled by microprobe analyses), and $CaCO_3$ was fused in a Pt-crucible previously equilibrated with a basaltic glass. Oxygen fugacity was adjusted to obtain a glass with a Fe^{3+}/Fe^{tot} ratio equal to 0.2. For homogeneity purposes, the first glass was finely ground and remelted. The greywacke is a natural amphibolite facies metagreywacke (CEV, [29]) composed of biotite+plagioclase+quartz. The fine-

Table 1
Bulk compositions

	MORB	Greywacke	Pelite
	TMB-7	CEV	CO821
SiO_2	51.0	70.4	64.4
TiO_2	2.0	0.7	0.8
Al_2O_3	14.7	13.1	18.1
FeO^{tot}	9.4	4.8	6.3
MnO	–	0.1	0.1
MgO	7.0	2.4	2.4
CaO	9.2	1.7	1.5
Na_2O	2.9	3.0	1.7
K_2O	0.9	2.4	2.6
H_2O	1.8	1.5	2.1
	100.0	100.0	100.0
H_2O^{phe}	0.4	1.1	1.2
H_2O^{free}	1.4	0.4	0.9

grained powder (<5 μm) was mixed with approximately 5 wt.% of a coarse-grained porous quartz (≈200 μm, not included in the bulk composition, Table 1). The porous quartz served as a melt trap at low melt percentages and although it transformed into coesite, it did not affect phase relations in the already SiO_2-saturated greywacke. The pelitic composition is an amphibolite facies natural metapelite (CO 821 [15]) composed of muscovite+biotite+plagioclase+garnet+staurolite+kyanite+chlorite+quartz and had the same coarse-grained porous quartz added. The natural H_2O contents of the metagreywacke and metapelite are 1.5 and 2.1 wt.%, respectively, bound in minerals such as muscovite, biotite, staurolite, and some retrograde chlorite. The H_2O content of the synthetic MORB was adjusted to lie in between (1.9 wt.% H_2O), such that all three bulk compositions had comparable water contents and were fluid-saturated at subsolidus conditions.

2.3. Phase compositions and mass balance

Mineral and melt compositions were measured with a Cameca SX50 electron microprobe, using silicate and oxide standards and 15 kV, 15 nA beam conditions for minerals. Conditions for measuring melt compositions are discussed in Section 3.3. As all phase compositions were measured by electron microprobe, phase proportions could be calculated by a least-squares procedure. Their errors were determined by Monte Carlo error propagation.

3. Experimental results

The MOR basalt, greywacke, and pelite were simultaneously brought to conditions of 3.5 to 7.5 GPa, 740 to 1180 °C (Table 2). From 3.5 to 7.5 GPa, the low-temperature mineral assemblages for the three compositions are remarkably comparable and correspond to a mixture of garnet+clinopyroxene+-phengite+coesite with or without kyanite or rutile (Fig. 2). This greatly simplifies high-pressure phase relations (Fig. 3). In all experiments, the metapelite is kyanite-saturated, the MORB kyanite-absent, and the greywacke has kyanite only at 1000 °C, 4 GPa. Although the eclogitic mineral assemblage remains identical with pressure, phase proportions (Fig. 2) and compositions necessarily differ in the three materials. The amount of phengite and coesite is smaller in the metabasalt, and clinopyroxene is less abundant and significantly more jadeitic in the metasediments. Nevertheless, the same mineral assemblage undergoes partial melting or dissolution in the three compositions (Figs. 4a, d, and g and 5a, d, and g). On the other hand, melt productivity and melting reactions at higher degrees of melting differ significantly.

3.1. Mineral compositions

Clinopyroxenes are mostly short prismatic and 5–20 μm in size (Figs. 4 and 5). They generally form compositionally homogeneous populations in each experiment. Clinopyroxenes were recalculated using a normalization scheme [30] that allows for vacancies in the M2-site. With increasing pressure, clinopyroxene becomes more jadeitic in composition (at 4.0→7.5 GPa: jad_{40}→jad_{55} in the basalt, jad_{65}→jad_{82} in the metasediments, Fig. 6). Apart from some minor Na_2O dissolved in the fluid, all Na_2O is incorporated in the jadeite component. Thus, the total amount of jadeite component is fixed by the bulk composition, and an increase in jadeite component in clinopyroxene must be accompanied by a decrease of the absolute amount of diopside component and an increase of garnet mode with pressure, as observed in all three compositions (Fig. 2). Clinoenstatite ($Mg_2Si_2O_6$), CaTs ($CaAl_2SiO_6$), and Ca–eskolaite ($\square_{0.5}Ca_{0.5}AlSi_2O_6$) are minor components in clinopyroxenes. Tetrahedral alumina was found to be insignificant and less than 0.02 Al^{IV} pfu in all experiments, except for the highest temperature experiments at 4 GPa in the metabasalt and the metapelite, in which Al^{IV} amounts to a maximum value of 0.07 apfu. Clinoenstatite component ranges between 4 and 9 mol% and increases systematically with temperature (Fig. 6) but does not appear to vary significantly with pressure. The proportion of Ca–eskolaite, i.e., vacancies on the M2-site, is significant in almost all experimental clinopyroxenes and amounts to 1–5 mol% in clinopyroxenes from the metabasalt. Higher values (4–9 mol%) are typical in the metasediments, and increase slightly with temperature. The sum of clinoenstatite and Ca–eskolaite component increases with temperature as shown in

Table 2
Run table and calculated phase proportions (wt.%)

	P (GPa)	*T* (°C)	*t* (h)		phe	glass	cpx	gar	coes	ky	rt
a203	3.5	740	125	B:	7.2	–	43.9	36.1	11.5	–	1.3
				G:	19.2	–	27.3	10.0	43.5	–	–
				P:	24.6	–	14.6	16.7	37.8	6.3	–
me36	4.0	790	141	B:	7.3	–	44.6	35.5	11.3	–	1.4
				G:	19.3	–	26.7	10.3	43.7	–	–
				P:	24.1	–	14.8	17.3	37.7	6.1	–
me35	4.0	850	96	B:	–	14.3	42.5	36.8	5.1	–	1.4
				G:	19.0	–	27.6	10.3	43.2	–	–
				P:	20.2	7.8	14.0	20.0	30.8	7.2	–
me32	4.0	900	60	B:	–	14.8	44.6	34.8	4.6	–	1.2
				G:	10.0	17.9	24.0	12.8	35.4	–	–
				P:	13.4	18.6	11.2	18.9	29.7	8.1	–
me40	4.0	950	122	B:	–	16.4	45.3	33.9	3.2	–	1.2
				G:	10.8	18.3	21.8	12.6	36.5	–	–
				P:	14.6	19.8	10.0	18.9	29.2	7.5	–
me33	4.0	1000	46	B:	–	28.8	38.3	32.5	–	–	0.4
				G:	–	57.9	–	16.4	25.6	0.2	–
				P:	–	49.2	–	20.7	20.1	10.1	–
me207	5.0	850	143	G:	22.8	–	26.7	10.0	40.5	–	–
				P:	24.4	–	14.3	18.0	35.8	7.5	–
me202	5.0	900	59	G:	16.0	9.1	25.4	13.0	36.5	–	–
				P:	17.7	12.3	9.0	21.1	31.4	8.3	–
me320	5.0	950	149	G:	–	31.6	18.1	19.2	31.0	–	–
				P:	–	42.2	–	24.9	22.1	10.9	–
me318	5.0	1000	74	G:	–	40.6	14.9	17.1	27.3	–	–
				P:	–	43.6	–	23.5	22.1	10.8	–
me107	5.5	810	51	B:	4.8	–	41.5	39.8	12.4	–	1.4
				G:	21.3	–	26.8	10.2	41.8	–	–
				P:	24.1	–	13.4	17.8	37.2	7.6	–
me204	6.0	900	143	G:	22.8	–	26.2	9.4	41.7	–	–
me219	6.0	900	124	P:	24.7	–	14.4	16.4	35.6	8.8	–
me96[a]	6.5	1050	71	B:	–	–	xx	xx	x	–	tr
				G:	18.4	–	24.0	12.9	44.8	–	–
				P:	–	–	xx	xx	xx	xx	–
me95[a]	7.3	1000	75	B:	–	–	xx	xx	x	–	tr
				P:	22.7	–	13.8	18.1	36.5	8.9	–
me90[a]	7.3	1120	30	B:	–	–	xx	xx	x	–	tr
				G:	–	–	xx	xx	xx	–	–
				P:	–	–	xx	xx	xx	xx	–
me97[a]	7.3	1180	26	B:	–	–	xx	xx	x	–	tr
				G:	–	–	xx	xx	xx	–	–
				P:	–	–	xx	xx	xx	xx	–
me106	7.5	910	45	B:	3.6	–	31.1	48.6	15.3	–	1.4
				G:	21.6	–	24.2	15.0	39.2	–	–
				P:	21.8	–	12.7	18.7	37.2	9.6	–

[a] Experiments without stable potassium phase could not be mass balanced, xx≥5 vol.%, x≤5 vol.%, tr: traces.

Fig. 6. This systematic increase, but a much more scattered variation of the two individual components, is probably due to the normalization scheme, in which clinoenstatite and Ca–eskolaite are the last components to be calculated and accumulate all analytical uncertainties of the atomic species.

Garnets are idiomorphic and vary in size from a few μm to about 30 μm. In the metabasalt, some

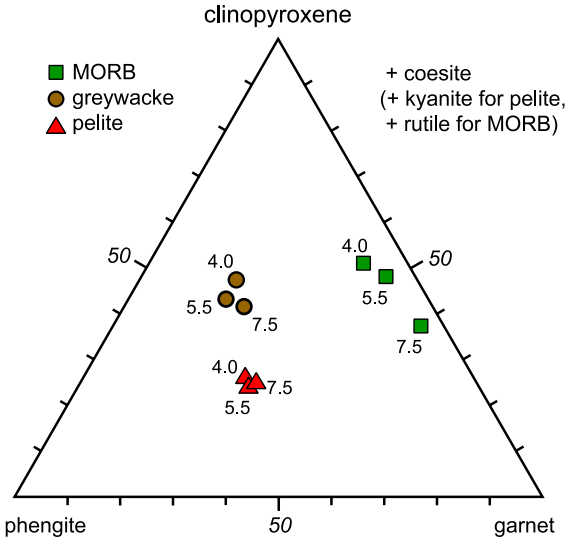

Fig. 2. Relative phase proportions in MORB (■), pelite (▲), and greywacke (●) at 4.0–7.5 GPa, 790–900 °C. Note that all three bulk compositions are composed of the same major minerals (of different compositions) and are saturated in SiO_2. Note the absence of a trend towards the garnet-corner in the pelitic composition, which is a result of majorite-free garnet to 7.5 GPa.

garnets are zoned with an Fe-rich core (Figs. 4a,b and 5a), which is attributed to fast crystallization of garnet from the glass starting material. Special care was taken to measure rim compositions. Garnets in the metagreywacke are relatively small (≤10 μm) and homogeneous, while garnets already present in the pelite starting material persist as cores (Figs. 4g,i and 5g,h). In the low-temperature, low-pressure experiments on the pelite, the garnet compositions farthest from the starting composition were selected, whereas in all other experiments, rims were large enough and average garnet rim compositions were obtained. Garnets in the metabasalt have higher grossular contents (23→33 mol%, Fig. 7) than in the metasediments (10→18 mol%), reflecting the higher Ca-content of the metabasalt composition. Majorite component in garnet is formed from garnets with 3.0 Si pfu through a negative *tschermak* exchange ($Mg+Si=Al^{VI}+Al^{IV}$). Such a majoritic component appears in significant amounts only in garnets from the basalt and the greywacke at ≥6.5 GPa and ≥5.5 GPa, respectively; the highest Si contents amount to 3.05 and 3.04 Si pfu, respectively. Majorite contents decrease with increasing temperature and become insignificant at 1120 °C (7.3 GPa). In metapelitic garnets, no significant majorite component is found even at 7.5 GPa. This is because the Al-side of the exchange vector is favored by a high chemical potential of Al in the bulk composition. Thus, a shift towards higher pressures of the majorite isopleths in the kyanite-saturated pelite is expected.

Phengites are generally small (≤15 μm), sometimes forming aggregates (Figs. 4 and 5). Not all experiments have sufficiently large grains to be analyzed by a defocused electron beam. This

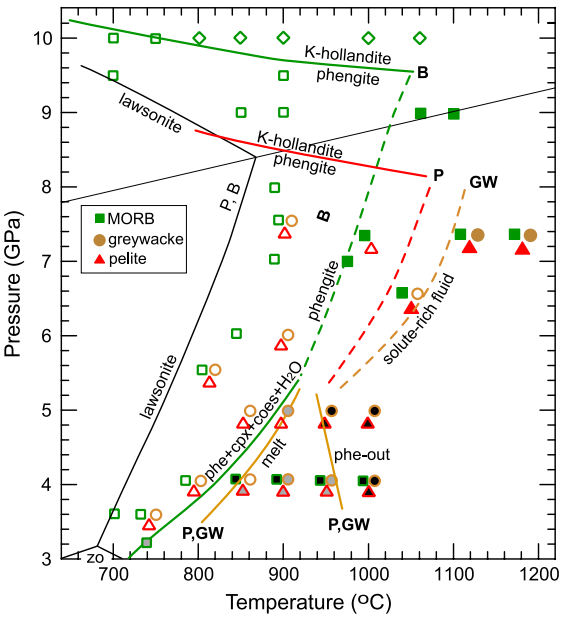

Fig. 3. Temperature–pressure diagram depicting experimental results and conditions of melting or dissolution of subducted crust. Experiments and phase boundaries involving potassium phases in MORB (green squares and diamonds), greywacke (brown circles), and pelite (red triangles) coded for potassium phases. Open symbols: phengite, grey fill: phengite+melt, black fill: melt, colored fill: potassium only in quench phases, green diamonds: K-hollandite ($KAlSi_3O_8$). Symbol triplets represent identical P–T conditions (see Table 2). The MORB experiments not listed in Table 2 are from [4,19]. The phengite to K-hollandite reaction for pelites is based on experiments detailed in Fig. 11. To 5 GPa, a classic melting sequence is observed. In the MORB, phengite disappears on the solidus. In the greywacke and pelite, phengite and melt coexist over a small temperature range. At ≥6.5 GPa, phengite disappearance does not result in a quenchable melt but in a supercritical melt. Most likely, melt was present but could not be recognized in all experiments at 4 GPa, 850 °C and at 5 GPa, 900 °C (see discussion in text).

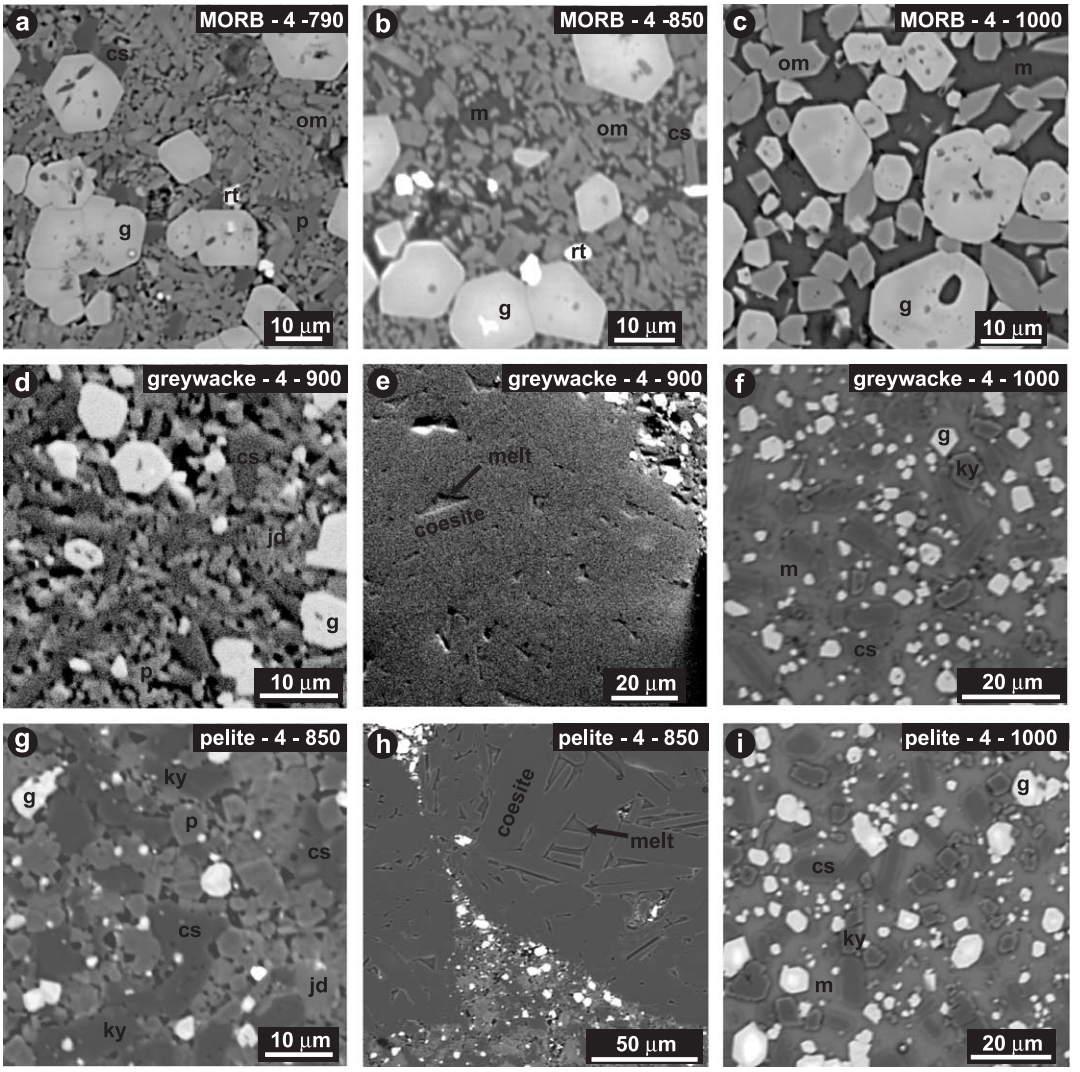

Fig. 4. BSE-images of melting series experiments at 4 GPa, 790–1000 °C in MORB (a–c), greywacke (d–f), and pelite (g–i). cs: coesite; g: garnet; jd: jadeitic clinopyroxene; ky: kyanite; m: melt; om: omphacite; p: phengite; rt: rutile. The left column shows the characteristic garnet–clinopyroxene–phengite–coesite±kyanite±rutile assemblage in each bulk composition. The middle column shows the first observed melt in each bulk composition. Note that, in experiments me32g (d and e) and me35p (g and h), melt is observable interstitially within the former "porous quartz" aggregate transformed to coesite but not detectable in the garnet+clinopyroxene+phengite+coesite±kyanite matrix of the greywacke (d) and pelite (g). Some of the interstitial material in panel (b) is glass but most of it is coesite. The right column shows the three bulk compositions at relatively high degrees of melting, i.e., after exhaustion of phengite and coesite in MORB and of phengite and clinopyroxene in the metasediments. In the pelite, residual starting material garnets cores are visible (e.g., lower left in panel (i)). The BSE-brightness is rutile>garnet>omphacite>phengite=jadetic cpx>melt>coesite=kyanite. In BSE-images of melt-rich experiments, kyanite grains can be distinguished from coesite by their thick white borders, e.g., panels (f) and (i).

resulted in K-losses in some analysis and either counting time or beam current was reduced in order to minimize them. The compositions of phengites are more scattered than those of garnets and clinopyroxenes, probably reflecting suboptimal analytical conditions. As expected, Si-contents in phengite increase with pressure, from 3.35 apfu at 4 GPa to 3.75 apfu at 7.5 GPa. Si-contents in

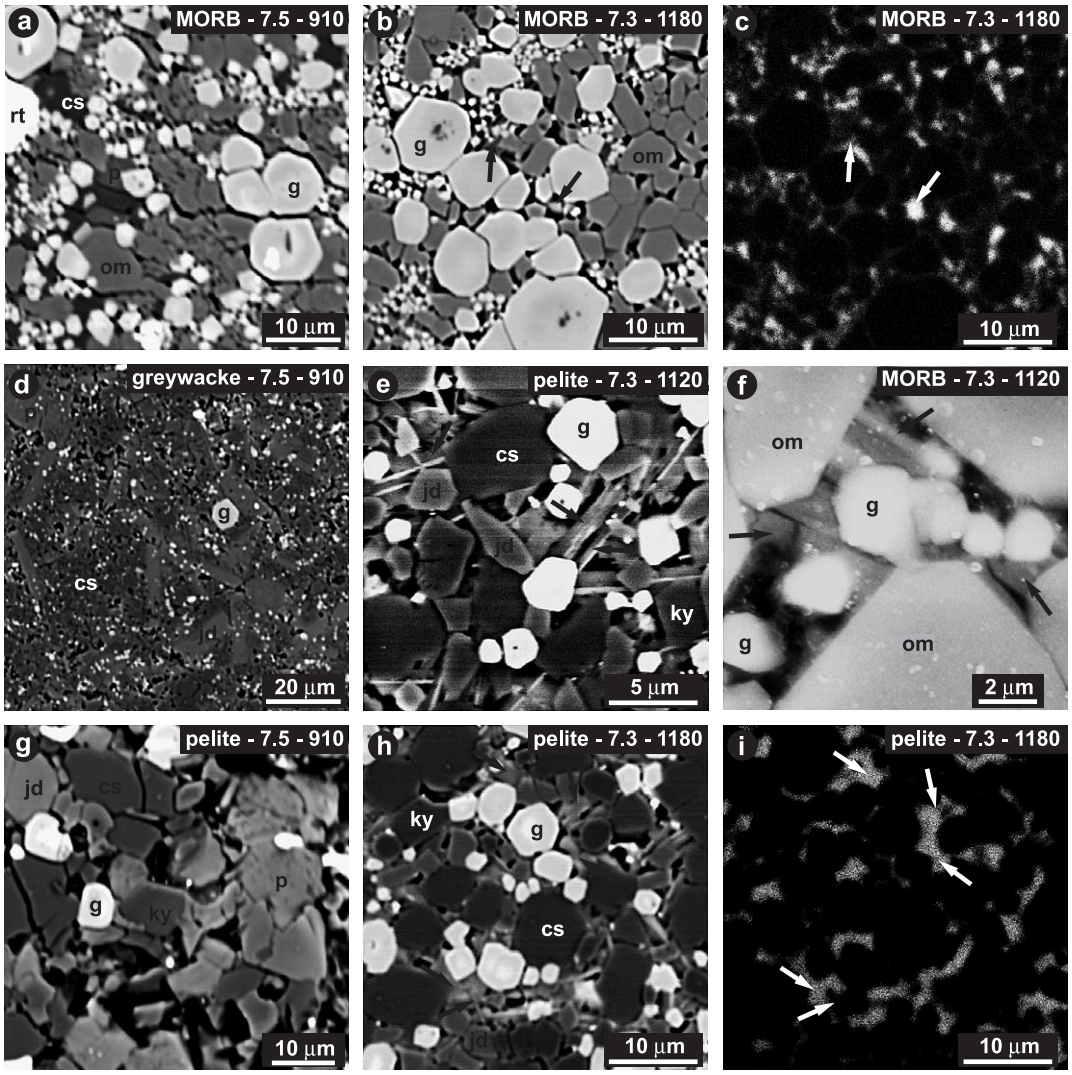

Fig. 5. BSE-images of dissolution series experiments at 7.3–7.5 GPa, 910–1180 °C in MORB (a, b, c, and f), greywacke (d), and pelite (g, e, h, and i). Abbreviations are as in Fig. 4. Left column: characteristic garnet–clinopyroxene–phengite–coesite±kyanite±rutile assemblage at 910 °C in each bulk composition. Jadeitic clinopyroxene and phengite (both intermediate grey) occur in panel (d) in about equal amounts, jadeitic clinopyroxene has the "sharper" grain boundaries. Middle and right column: garnet+clinopyroxene+coesite±kyanite assemblage in MORB and pelite coexisting with an unquenchable supercritical melt. (b and c) Garnet+omphacite+coesite in MORB without an equilibrium potassium phase but with potassium distributed interstitially, panel (c) is the K–Kα element distribution map corresponding to panel (b). (h and i) Garnet+omphacite+coesite+kyanite in pelite without an equilibrium potassium phase but with abundant quench phases and the characteristic interstitially distribution of potassium, panel (i) is the K–Kα element distribution map corresponding to panel (h). All phases that appear to be in the background in panels (e) and (h) are quench phases. (e and f) Details of zones rich in quench-phases in pelite and MORB. Arrows indicate some of quench phases which are mostly quartz/coesite or K–Al–Si–rich phases. Note the large intergranular distances (also already at 910 °C) which are often partly filled by minuscule quench phases. The BSE-brightness is rutile>garnet>omphacite>phengite=jadetic cpx>coesite=kyanite.

phengite in the kyanite-saturated metapelite are systematically lower (and Al-contents higher) than in the other two bulk compositions, again pointing out a shift of tschermak-exchange equilibria towards the Al-rich side. In all experiments, phengite is the most magnesian phase ($X_{Mg}^{phe} > X_{Mg}^{cpx} \gg X_{Mg}^{gar}$) with

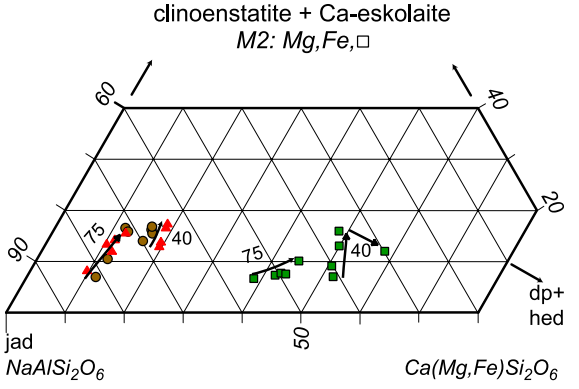

Fig. 6. Clinopyroxene compositions in MORB (green squares), greywacke (brown circles), and pelite (red triangles) at 4 and 7.3–7.5 GPa. Triangle: jadeite–dioside–clinoenstatite+Ca–Eskaloite ($NaAlSi_2O_6$–$Ca(Fe,Mg)Si_2O_6$–$(Mg,Fe)_2Si_2O_6$+$Ca_{0.5}\square_{0.5}AlSi_2O_6$). Note that Na/Ca ratios in clinopyroxenes at 4 GPa do not change strongly when crossing the solidus. At high degrees of melting in the MORB, jadeite component in clinopyroxene decreases. Arrows indicate increasing temperature. (For interpretation of the references to colour in this figure legend, the reader is referred to the web version of this article).

X_{Mg}=0.84–0.9 in the MORB and 0.64–0.78 in the metasediments.

3.2. Melting at 4 and 5 GPa

At 4 GPa, phengite is no longer present at 850 °C in the basalt (Fig. 4b) and 14 wt.% melt were produced (Table 2 and Fig. 8). In the pelite, a small amount of melt (calculated to 8 wt.%) was observed in the coesite-aggregate (Fig. 4h), while melt was undetectable in the reminder of the capsule (Fig. 4g). At the same temperature, melt could not be detected in the greywacke; however, a small amount of melt (<3%) is suspected because even the small amount of free fluid entrapped in the capsule should cause a small degree of fluid saturated melting. The basalt has the largest amount of fluid below the solidus (i.e., 1.4 wt.% unbound H_2O; Table 1), followed by the pelite and greywacke (0.9 and 0.4 wt.% H_2O, respectively), and thus should produce proportional amounts of melt on crossing the wet solidus. At 900 °C, melting is observed in all three compositions. Phengite coexists with 18–20 wt.% melt in the metasediments at 900–950 °C (Fig. 8). Mass balance calculations indicate that the mode of garnet increases upon crossing the solidus in all three compositions. However, this increase (+1.2 to +2.7 wt.%) is small at 4 GPa and a eutectic melting reaction such as:

$$\text{phengite} + \text{clinopyroxene} + \text{coesite} + \text{fluid} = \text{melt} \quad (1)$$

is held responsible for the first appearance of melt in all three compositions. Upon further increase in temperature, clinopyroxene and phengite both disappear between 950 and 1000 °C in the metasediments (Fig. 4f,i), resulting in 49 and 58 wt.% melt in the greywacke and pelite (Fig. 8). Mass balance calculations indicate the following peritectic melting reaction:

$$\text{clinopyroxene} + \text{phengite} + \text{coesite} = \text{melt} + \text{garnet}, \quad (2)$$

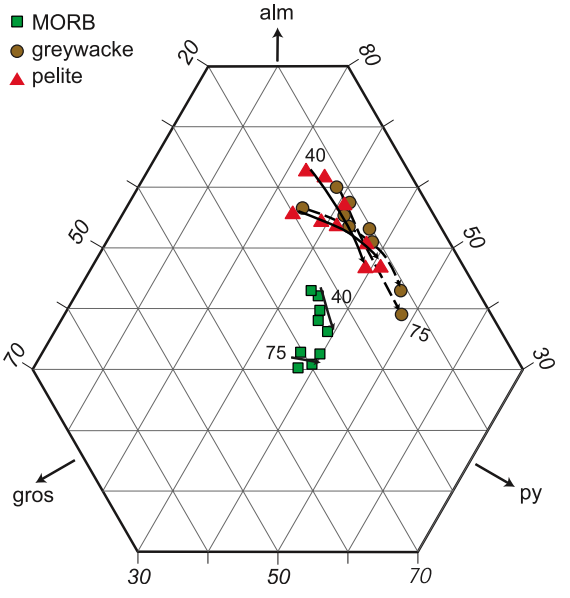

Fig. 7. Garnet compositions in MORB (green squares), greywacke (brown circles), and pelite (red triangles) at 4 and 7.3-7.5 GPa. Arrows indicate increasing temperature. Note the similar and low grossular component in the metasedimentary compositions. The proportion of grossular in garnet generally increases with pressure. (For interpretation of the references to colour in this figure legend, the reader is referred to the web version of this article).

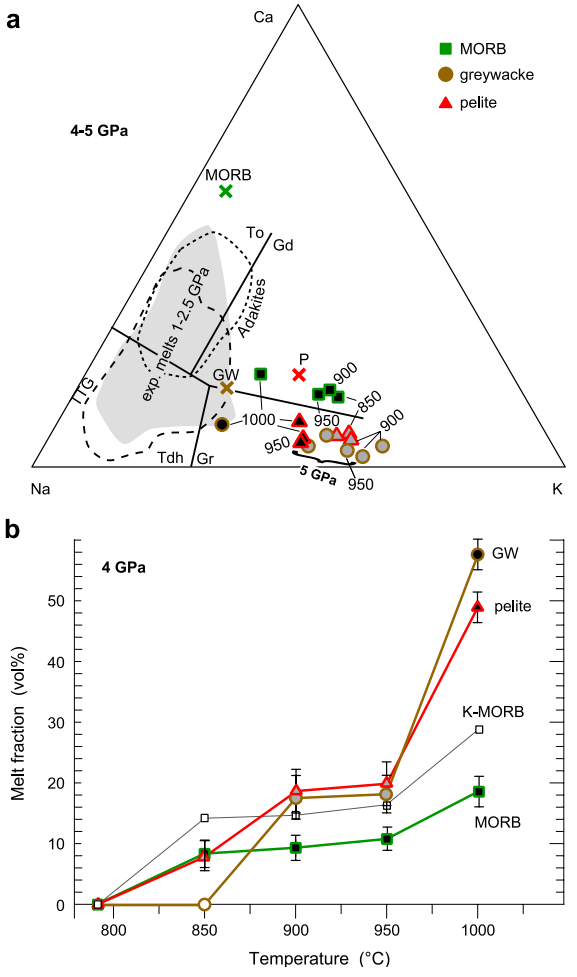

Fig. 8. Melt composition at 4 and 5 GPa (a) and melt productivity at 4 GPa (b). (a) Melt compositions at 4 and 5 GPa are relatively Ca-poor and K-rich and represent potassic, slightly peraluminous granites. The 5 GPa melts have lower Ca-contents than the 4 GPa melts. Crosses: bulk compositions. Experimentally determined melt compositions from basalts at 1–2.5 GPa (grey field) correspond well to adakites (field limited by short dashed line) and members of the trondhjemite–tonalite–granodiorite suite (TTG, field limited by long dashed line) both interpreted as slab-derived melts (fields modified after [50]). The melt compositions obtained at 4 GPa are far more potassic due to the effect of pressure on Na-partitioning between cpx and melt. (b) Melt fractions with their errors as calculated from mass balance. Black open small squares represent melt fractions calculated for the experiments (performed on a K-enriched MORB, Table 1), while larger green squares are melt fractions recalculated for MORB with 0.4 wt.% K_2O. (For interpretation of the references to colour in this figure legend, the reader is referred to the web version of this article).

which causes a large increase in melt fraction over a relatively narrow temperature range. At 5 GPa, melting reactions in the greywacke and metapelite are similar, but the minimum melting reaction has a more pronounced peritectic character (i.e., resulting in +3.0 and +3.2 wt.% garnet, respectively), phengite is exhausted earlier (950 °C in the greywacke, before clinopyroxene), and coesite persists to >1000 °C.

In the basalt, only a small increase of the melt proportion, from 14 to 16 wt.%, is observed between 850 and 950 °C (Table 2 and Fig. 8). At 1000 °C (Fig. 4c), the jadeite component in clinopyroxene decreases drastically (down to jad_{30}; Fig. 6), coesite is finally consumed, and the amount of melt increases to 29 wt.% by the reaction

$$\text{clinopyroxene} + \text{coesite} = \text{melt} + \text{garnet}. \quad (3)$$

In summary, at 4–5 GPa, classical melting behavior is observed for the three bulk compositions.

3.3. Melt compositions at 4 and 5 GPa

In the metabasalt at 850 and 900 °C, melt formed small pools that could be analyzed with a 3-μm-diameter electron beam. With this relatively small beam diameter, some sodium and potassium is lost due to thermal diffusion. Thus, Na_2O- and K_2O-contents of the melts at 850–900 °C in the basalt were recalculated from mass balance: first, the amount of melt was calculated from the other oxides, then, Na_2O and K_2O in the melt was calculated in order to fit the bulk composition. For both oxides, a +10 to +20 wt.% relative correction was obtained. Melt pools in the MORB at 950 and 1000 °C were large enough for the use of a 5- to 10-μm-diameter beam and could be directly measured. Melt compositions in the metasediments were directly measured with a defocused electron beam, as relatively large melt pockets formed in the former porous quartz that transformed into coesite aggregates (Fig. 4l,h). Melt pockets close to the aggregate rims have the same composition as in the center, suggesting that the trapped melt was equilibrated with the bulk of the sample. Mass balance of the experiments with larger melt pools yielded a deviation of calculated Na_2O and K_2O from bulk Na_2O and K_2O of +1 to −7 wt.% relative, indicating insignificant Na or K loss during analyses.

Initial melts are metaluminous to slightly peraluminous potassic Si-rich granites with K/Na ratios of 1.4–2.0 (Table 3 and Fig. 8). Melt compositions in all three bulk compositions at 900 °C (4 GPa) are strikingly similar for the MORB, greywacke and pelite. The only significant differences between the three melt compositions at 900 °C are the higher CaO and MgO contents in the potassic granite derived from the MORB, reflecting its relatively CaO- and MgO-rich bulk composition. The melt compositions are remarkable in that jadeite component in clinopyroxene does not partition preferentially into the melt at temperatures up to 1000 °C. Jadeite contents in clinopyroxenes forming 100 °C above the solidus remain almost unchanged compared to subsolidus conditions, and are as high as $jad_{63–68}$ in the metasediments and $jad_{36–41}$ in the metabasalt. The strongest partitioning of Na into clinopyroxene is observed just above the solidus (4 GPa: $D_{Na}^{cpx/melt}$=2.2–2.4 in the basalt, 3.7–4.0 in the metasediments). A significant decrease of $D_{Na}^{cpx/melt}$ occurs at 1000 °C in the basalt (to $D_{Na}^{cpx/melt}$=1.3). $D_{Na}^{cpx/melt}$ decreases only slightly with temperature in the metasediments, in which clinopyroxene melts out at 1000 °C, leaving a melt coexisting with garnet, kyanite, and coesite with the bulk K_2O/Na_2O ratio.

3.4. Dissolution regime at 6.5–7.5 GPa

At pressures higher than 5 GPa, phengite disappears without producing a quenchable silicate melt (Fig. 5). In these experiments, potassium is concentrated along grain boundaries (Fig. 5c,i; this is also observable when phengite is still present). The run products display a peculiar behavior under the electron beam of the microprobe. When focusing the electron beam on a potassium-rich intergranular space, K–Kα count rates decrease within a few seconds to less than a quarter of their initial value and a deposit forms around the spot of analysis. This deposit is clearly visible in BSE- and SE-images and qualitative measurements of the deposit compositions demonstrate a K- and Al-rich character.

With increasing temperature, the proportion of phengite decreases, and then phengite completely disappears, first in the MORB, then in the pelite, and finally in the greywacke (Fig. 2). Instead, quench phases interstitial between the texturally equilibrated phases become abundant (Fig. 5e, f, and h). Generally, the quench phases are neither large enough, nor sufficiently polished to obtain reliable microprobe analyses. In most cases, analyses are contaminated by neighboring phases, and their identity needs to be taken

Table 3
Melt compositions at 4 and 5 GPa

P–T	MORB				Greywacke						Pelite					
	850–4	900–4	950–4	1000–4	900–4	950–4	1000–4	900–5	950–5	1000–5	850–4	900–4	950–4	1000–4	950–5	1000–5
SiO_2	73.00	73.41	73.14	69.50	75.18	73.58	70.43	73.96	71.03	71.86	76.80	76.62	75.00	71.40	72.02	71.55
TiO_2	0.43	0.27	0.64	2.89	0.42	0.59	1.01	0.44	0.28	0.55	0.29	0.37	0.91	1.20	0.39	0.48
Al_2O_3	13.65	13.65	14.06	15.25	13.45	14.30	15.55	13.02	15.58	15.77	13.42	13.38	13.57	14.66	14.98	15.27
FeO	0.95	0.91	1.15	2.51	0.84	0.90	1.60	1.22	0.88	1.07	0.81	0.77	1.14	2.03	1.14	1.33
MnO	0.00	0.00	0.00	0.00	0.03	0.00	0.00	0.08	0.07	0.02	0.01	0.03	0.02	0.01	0.01	0.00
MgO	1.10	1.04	0.88	0.53	0.28	0.42	0.80	0.19	0.30	0.28	0.32	0.20	0.22	0.61	0.28	0.32
CaO	2.33	2.09	2.06	2.51	0.56	0.94	1.41	0.27	0.52	0.64	0.85	0.65	0.87	1.37	0.87	0.93
Na_2O	2.81	2.76	2.81	3.30	2.30	3.19	5.12	3.08	3.48	3.71	2.36	2.40	2.68	3.45	4.00	3.90
K_2O	5.73	5.87	5.26	3.52	6.94	6.08	4.08	7.74	7.87	6.11	5.12	5.58	5.59	5.27	6.31	6.20
	100.0	100.0	100.0	100.0	100.0	100.0	100.0	100.0	100.0	100.0	100.0	100.0	100.0	100.0	100.0	100.0
$tot^{measured}$	86.6	86.4	89.8	91.9	89.2	88.9	97.1	92.7	96.0	96.3	88.0	87.6	90.1	95.9	95.8	94.8
$H_2O^{calculated}$	12.5	12.2	11.0	6.3	8.4	8.2	2.6	8.0	4.6	3.5	15.4	11.3	10.6	4.3	5.1	5.0
K/Na (M)	1.4	1.4	1.2	0.7	2.0	1.3	0.5	1.7	1.5	1.1	1.4	1.5	1.4	1.0	1.0	1.1
Al/(K+Na+2Ca)	0.91	0.93	1.00	1.11	1.09	1.06	1.01	0.94	1.03	1.14	1.22	1.20	1.13	1.06	1.00	1.03
F (wt.%)	14.3	14.8	16.4	28.8	17.9	18.3	57.9	9.1	31.6	40.6	7.8	18.6	19.8	49.2	42.2	43.6
*F** (wt.%)	8.4	9.4	10.9	18.7	–	–	–	–	–	–		–	–	–	–	–

$H_2O^{calculated}$: concentration of H_2O in melt calculated from the proportion of melt (by mass balance) and the proportion of bulk H_2O not stored in phengite.

into account when evaluating the analyses. Nevertheless, the semiquantitative analyses reveal that the quench phases are either a SiO_2-polymorph or mostly consist of K_2O, Al_2O_3, and SiO_2, with $K_2O \gg Na_2O$. The amounts of Na_2O and FeO are low in quench products (<1 wt.%), which contain almost no CaO nor MgO. Thus, the inferred, unquenchable interstitial liquid predominantly mobilizes K, Al, and Si. The observed disappearance of phengite with temperature is consistent with a chemical continuum in the fluid/melt phase and thus suggests that the solvus between fluid and melt is closed at these pressures (see Discussion).

The maximum amounts of K_2O and H_2O in the unquenchable liquid can be established from the K_2O:H_2O mass ratios in the starting materials. K_2O:H_2O mass ratios of 33:66, 55:45, and 62:38, in the MORB, pelite, and greywacke, respectively, indicate that the unquenchable phase contained 66 wt.% H_2O in the basalt and 38 wt.% H_2O in the greywacke at the temperature of complete disappearance of phengite at most (i.e., if no other solute than K_2O was present in the unquenchable phase). These numbers overestimate the concentrations of K_2O and H_2O in the liquid phase, as other chemical species dissolve. Any microprobe measurement indicated less than 55 wt.% K_2O and more than 45 wt.% SiO_2+Al_2O_3 (normalized to 100%). Thus, it appears reasonable to consider that other oxides were dissolved in the unquenchable liquid phase at least in equal amount to K_2O. From such considerations, it is speculated that the amount of H_2O in the unquenchable phase was less than 30 wt.%. This is not far from the 25 wt.% H_2O dissolved in a granitic melt at 3 GPa [31]. In summary, at pressures greater than 5 GPa, dissolution probably plays a major role in the breakdown of phengite and a classical melting process may cease to operate.

4. Discussion of the melting relations (≤5 GPa)

4.1. Melting sequence

Melt productivities for MORB with 0.4 wt.% K_2O, greywacke, and metapelite at 4 GPa are compared in Fig. 8. Data obtained on the K-rich MORB (our starting material) were used to retrieve the melt and phengite proportions in average MORB. This calculation was performed first by subtracting the adequate amount of phengite or melt from the original K-rich bulk composition such that K_2O is completely bound in phengite or melt. Garnet, clinopyroxene, coesite, and rutile are then mass balanced with the reminder of the bulk, and an amount of phengite or melt equivalent to 0.4 wt.% bulk K_2O is then calculated back into the mode.

Mineral and melt proportions at 4 GPa are presented in Fig 9. The most striking feature in this melting series is the observation of the largest amount of melt in the MORB at 850 °C (Fig. 8). All three compositions have low and almost identical H_2O contents (1.5 to 2.1 wt.%, Table 1). However, a nearly identical bulk-H_2O in the starting material caused the three bulk compositions to have different amounts of free fluid, i.e., H_2O unbound in hydroxylated phases, when composed by phengite+garnet+-clinopyroxene+coesite±kyanite. The MORB had 1.4 wt.% structurally unbound H_2O, the pelite 0.9 wt.%, and the greywacke 0.4 wt.%, respectively. The melting sequence observed in the three bulk compositions can be explained if the small but significant amounts of free fluid are taken into account: (i) The largest amounts of free fluid are present in the basalt and then pelite where fluid-saturated melting forms a detectable amount of melt and causes phengite to disappear in the basalt between 790 and 850 °C. This corresponds to a melt productivity in the assemblage phengite−clinopyroxene−garnet−quartz proportional to the amount of fluid present at the solidus. (ii) Within the interval 790–900 °C, significant melting occurs in the metasediments, resulting in about 18 wt.% melt (4 GPa). To temperatures of 1000 °C, melt productivity depends then largely on the amount of phengite. (iii) Melt proportions increase only slightly in metasediments until phengite+clinopyroxene disappear leading to as much as 50 wt.% potassic granite melt over a short temperature interval (950–1000 °C, 4 GPa). (iv) Omphacitic clinopyroxenes in basalt are stable to higher temperatures (>1000 °C) than jadeitic clinopyroxenes in metasediments. Thus, the discontinuous increase of melt proportion in basalt due to incongruent melting of clinopyroxene is displaced to higher temperatures.

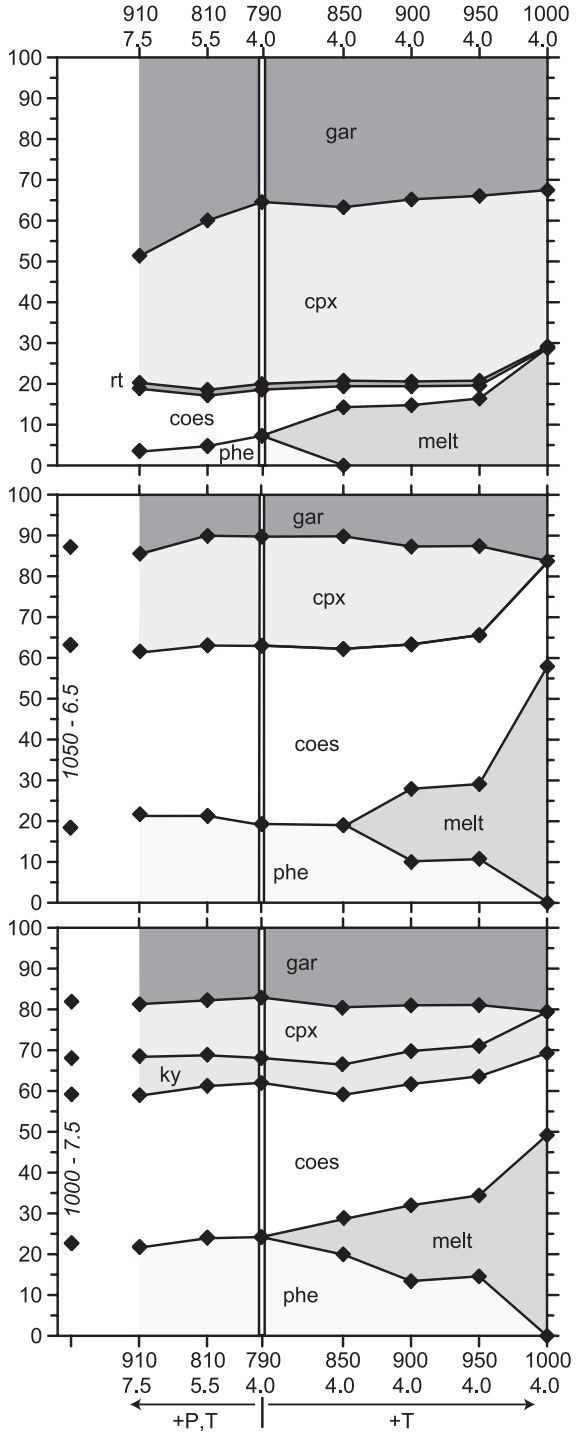

Fig. 9. Calculated phase proportions in MORB (top), greywacke (middle), and pelite (bottom). Towards the right side, temperature increases (at 4 GPa), whereas pressure increases along a subduction geotherm to the left side. The mineral proportions are calculated for a 'fluid-absent' situation. In the presence of fluid (as in the experiments) phengite would be dissolved incongruently. The greywacke contains <1 wt% kyanite at 4 GPa, 1000 °C.

4.2. Comparison to previous studies

Our experiments constrain the minimum melting of phengite+clinopyroxene+coesite+fluid (1) to temperatures between 790 and 850 °C at 4 GPa and 850–900 °C at 5 GPa. This is in excellent agreement with the wet pelite solidus determined up to 3 GPa by Nichols et al. [32] and with the K_2O-added (1.4 wt.% K_2O) MORB solidus at 2.85 GPa [33] (Fig. 1). The location of the phe+cpx+qtz/coes+H_2O solidus is also in agreement with the granite solidus determined to 3.5 GPa [31]. In the latter study, the subsolidus assemblage above 2 GPa is also phengite+jadeite+coesite. In addition, our location of the solidus is consistent with the studies in the synthetic KCMASH-system ([34] at ≥2 GPa, and [35] at <2 GPa) because the minimum solidus in the latter Na_2O- and FeO-absent system is about 50–70 °C higher than in our complex natural system. However, the solidus compiled from [32] and this study is incompatible with the solidi found by Johnson and Plank [14] at 2 to 4 GPa, and by Domanik and Holloway [12], Ono [7], and Irifune et al. [13] at higher pressures. The solidus determined by Johnson and Plank [14] is located at least 110 to 150 °C higher than in this and other previous studies. Possible explanations are that relatively small amounts of melt were not detected by Johnson and Plank, or that some experiments, critical for the location of the solidus, lost fluid leading to the determination of a fluid-absent solidus.

5. Discussion of phengite dissolution in a supercritical melt ($P \geq 6.5$ GPa)

5.1. Sequence of phengite dissolution

The sequence of phengite dissolution can be readily explained by the different ratios of structurally unbound H_2O to phengite in the different starting materials. The MORB has a H_2O:K_2O bulk weight

ratio of 2.0, resulting in a molar ratio of unbound H_2O to phengite of 4:1. This is the highest amount of free H_2O and the lowest amount of phengite compared to pelite and greywacke which have H_2O:K_2O wt-ratios of 0.81 and 0.63, and molar ratios of unbound H_2O to phengite of 0.91 and 0.44, respectively. Consequently, when the solubility of potassium in the unquenchable liquid phase increases with temperature, phengite will be first completely dissolved in the MORB, followed by the pelite and then the greywacke. This corresponds to the sequence of dissolution observed in the experiments with increasing temperature.

5.2. The critical curve of the melt–fluid solvus and supercritical melts

In the experiments, contrasted melting/dissolution behavior was observed as a function of pressure in all three chemical systems: at pressures to 5 GPa, phase relations can be interpreted in terms of classical melting, while at higher pressures, continuous dissolution plays an important role. There, the progressive disappearance of phengite, the presence of an unquenchable potassium-rich liquid phase, and the difficulty of identifying a melt indicate the closure of the solvus between a low-density aqueous phase, commonly referred as 'fluid', and a high-density hydrous silicate phase, commonly referred as 'melt'.

Phase relations associated with the presence and closure of a solvus in heterogeneous equilibria were studied in detail by Ricci ([1] p. 65/70). Boettcher and Wyllie [22] also illustrated the consequences resulting from the closure of the solvus between aqueous fluid and siliceous melt in a ternary system. Here we consider the implications of such a situation on phase relationships in a simple model system A-H_2O which generates all phenomena necessary to understand natural systems. This system involves an aqueous fluid Fl, two hydrous minerals H1 and H2, and a silicate melt M. For a closer match to real situations, the anhydrous minerals A′ to A‴ and two phase transitions (A′ =A″, A″=A‴) are considered. A theoretical *P–T* projection and related T–X sections at three pressures are shown in Fig. 10 which is a direct extension of the phase relation analysis proposed by Vielzeuf and Schmidt [6] modified to include the closure of the solvus between melt and fluid at high pressures.

In Fig. 10, phase relations below *P*=4 (in arbitrary units) correspond to a classical melting situation. To higher pressures and temperatures (e.g., T–X section at *P*=6, Fig. 10), a critical solution point k appears on top of the solvus between fluid and melt, where the composition of the fluid and melt coincide. The projection of such points on a *P–T* surface generates a critical solution curve (shown as a straight pointed line, Fig. 10). At pressures and temperatures above this line, the aqueous fluid (Fl) and the hydrous silicate melt (M) are no longer separate phases and are replaced by a supercritical melt (SM). In the *P–T* diagram, the intersection of the critical curve with the hydrous solidus (H1+Fl=M) generates a singular endpoint SCP (or critical solution point[1]) where the fluid-saturated solidus vanishes, without metastable extension. At pressures above the critical line, there is a continuity from a low temperature "fluid" to a high temperature "melt". It should be pointed out that it is the chemical continuum between pure H_2O and a dry silicate melt which is the characteristic of a supercritical melt.[2] This chemical continuum implies a continuum in physical properties of liquids between H_2O and A, but this situation does not imply that dry or almost dry silicate melts with their specific physical properties do not exist. This fact becomes important for a consistent interpretation of existing experiments on metasediments.

The reaction H1=A″+M is a typical fluid-absent reaction. Unlike the hydrous solidus, its intersection with the critical curve does not generate any singular point. Along this reaction, with increasing pressure, the composition of the melt changes continuously even across the critical curve where melt turns into a supercritical melt. Two consequences of the phase diagram in Fig. 10 are necessary for understanding natural processes at pressures above the second critical endpoint and are illustrated in the T–X

[1] For such singular endpoints, Boettcher and Wyllie [22] used the term second or upper critical end-point.

[2] We employ the term "supercritical melt" (which is only applicable to systems with at least two components) to qualify liquid solutions beyond the closure of the fluid–melt solvus. This is in order to distinguish against "supercritical fluid", which (i) is also applicable to unary systems describing a change of structure but not of chemical composition at the termination of the liquid–gas curve, and which (ii) describes any geological fluid beyond a few 100 bar and °C.

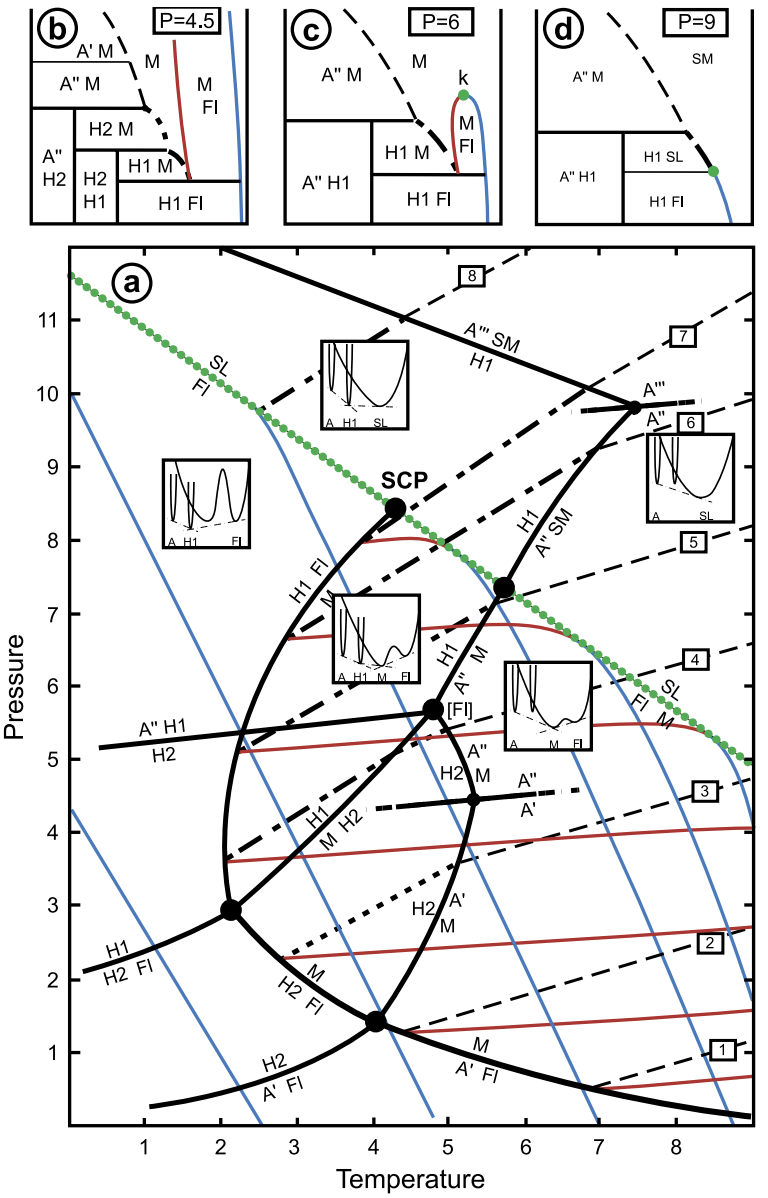

Fig. 10. Simplified binary system A-H_2O illustrating phase relations and H_2O-isopleths with closure of the fluid–melt solvus, fluid-saturated, and fluid-absent melting reactions. Arbitrary P and T units. A′ through A‴ are anhydrous phase, H2 and H1 are hydrous phases and represent analogues to biotite and phengite, respectively. Fl: fluid; M: melt; SM: supercritical melt. H_2O-isopleths: blue lines, fluid; red lines, melt coexisting with fluid; dash-dotted lines, melt or SM coexisting with H1; dotted line, melt coexisting with H2; dashed line, melt coexisting with A′ through A‴. The positions of H1 and M on the x-axis in the T–X diagrams (b–d) correspond to phengite and hydrous melt at 3 GPa which have 17 and 55 mol.% H_2O, respectively. A supercritical melt forms beyond the crest of the fluid–melt solvus (k in panel (c)). Alignment of these critical points in P–T result in a critical curve at which H_2O-isopleths of fluid and melt converge (pointed line in panel (a)). The intersection of this curve with the fluid-saturated solidus generates its critical endpoint SCP. At lower temperatures, a critical curve can still be defined by the metastable existence of melt (see G–X diagram). The five inserted G–X diagrams (Gibbs free energy vs. composition) illustrate these changes at high pressure. Note that the fluid-absent melting reaction of H1 has a continuation extending beyond the critical curve (a) and that any bulk composition between A and H1 (i.e., a classical “fluid-absent” assemblage) will produce a supercritical melt at a defined temperature also at pressures above the termination of the wet solidus.

diagrams. First, the temperature of disappearance of the hydrous phase H1 (phengite in our experiments), depends (at constant P) on bulk composition for "excess H_2O" bulk compositions located between H_2O and H1, high H_2O-contents resulting in complete dissolution of H1 at relatively low temperatures. Secondly, any bulk composition situated between H1 and A will generate a supercritical melt and have H1 disappearing through a discontinuous "fluid-absent" reaction at a defined temperature (for each P). Whether this liquid will be quenchable depends on its H_2O-content (which in turn depends on the stoichiometry of this peritectic reaction).

Thus, at pressures greater than SCP, the wet solidus does not exist, but the 'fluid-absent' solidus can be crossed and may lead to quenchable liquids with low H_2O contents. It should be emphasized that there is no direct relation between the ability of a melt to quench and the critical curve. Being above the critical curve does not mean that all melts are rich in H_2O, and thus the critical curve is not necessarily the end of quenchable melts.

The first experimental evidence of complete miscibility between silicate melts and H_2O at high pressures and temperatures and the termination of the solidus was reported by Kennedy et al. [25] in the system SiO_2–H_2O (SCP at 1.0 GPa, 1080 °C). Other cases in various systems, including albite–quartz–H_2O (SCP at 1.5 GPa, 670 °C), have been observed [22,36], inferred [23,37], or have been assumed to occur near 12 GPa in the MgO–SiO_2–H_2O system [24]. In this context, it should be pointed out, that Shen and Keppler [37] and Bureau and Keppler [23] observed the closure of the solvus between fluid and melt and a portion of the critical curve, but not the intersection of the critical curve with the fluid-saturated solidus.

5.3. Towards a high-pressure phase diagram for metasediments

The continuous dissolution of phengite indicates that, at 6.5 GPa, the solvus between fluid and melt is closed for basaltic and pelagic bulk compositions. The H_2O-contents in this study allowed a complete dissolution of phengite between 1000 and 1100 °C. Higher H_2O-contents would result in lower temperatures for phengite disappearance, and fluid-absent systems should result in the extension of phengite stability to higher temperatures.

The present experiments on the basaltic composition are consistent with previous experiments by Schmidt on MORB with 2 wt.% H_2O [19] but not with the previous interpretation: a wet solidus was drawn to 10 GPa based on the absence of phengite and the presence of quench material located between grain boundaries. Above 5 GPa, a quenched melt was not observed [19] and reexamination of these experiments shows the same dissolution phenomena as in this study, with a potassium-rich quench phase concentrated at grain boundaries.

Numerous experimental studies on high pressure melting in metapelitic systems are available. The proposed phase diagrams are mutually inconsistent at high pressure [7,12,13] and incompatible with experiments from pressures below 3.5 GPa [32,33]. The comparison of the present experiments to reactions drawn in previous studies on metasediments [7,12] or directly relevant bulk compositions [13] also show significant discrepancies. At a first glance, the high-pressure melting reactions compiled in Fig. 1 appear contradictory. However, a coherent picture emerges when the results of individual experiments in the different studies are compared (Fig. 11).

The upper pressure stability of phengite and formation of K-hollandite in metapelitic compositions [7,12,13] are consistent only if the following changes are made: (i) The "non-phase-separated experiments", i.e., those without extreme zonations in the capsules of Domanik and Holloway [12] are considered. (ii) The so-called OCD–muscovites (deficient in octahedral cations) [12] are interpreted as quench products. (iii) The impure "orthoclase" by Irifune et al. [13] is a phengite: Irifune et al. argued that they could not obtain a pure analysis of this hypothetical orthoclase due to its small grain size and contamination of the analysis by neighboring phases. However, the relevant analysis (their Table 3, MA-687-2, or) is a perfect phengite with 3.62 Si pfu. (iv) Irifune et al. [13] proposed, by analogy to simple K_2O–Al_2O_3–SiO_2–H_2O systems, a stability field of wadeite ($K_2Si_4O_9$). However, this phase was not encountered and there is yet no indication that such a field exists in natural bulk compositions.

The fact that phengite is completely dissolved in a few weight percent (wt.%) H_2O at pressures above 6

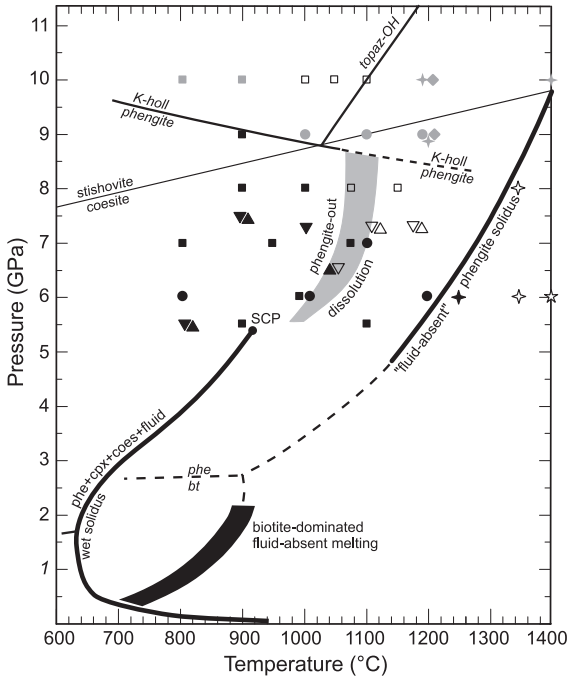

Fig. 11. Integrated phase diagram for sediment melting based on a compilation of high-pressure experiments on metasediments. Pelites: upwards pointing triangle (this study); circles and five-pointed star [7]; squares and diamonds [12]. Greywacke: downward pointing triangle (this study). Four-pointed stars represent an average continental crust composition with FeO substituted by CoO [13]. The reported experimental results are: black symbols: phengite, no melt; open symbols: melt or quench material present; grey filled symbols: K-hollandite. Symbols that stand close to each other represent experiments at the same conditions. The stippled line gives a schematic fluid-absent solidus and biotite to phengite reaction. Note that the dissolution temperature of phengite depends on the K_2O:H_2O bulk ratio, the grey band designated here corresponds to the dissolution temperature at about 2 wt.% H_2O in metapelites/metagreywackes. The results on the phengite and topaz-OH reactions are coherent and the observed dissolution temperature (grey area) of phengite is in agreement with most other experiments. The two experiments at 6 GPa, 1200 °C and at 5.5 GPa, 1100 °C can be reconciled with the other experiments if it is assumed that the former were fluid-absent and thus, phengite stabilized to temperatures of the fluid-absent melting reaction. The pressure-limit of the wet solidus at the second critical end-point near 5 GPa and the formation of quenchable melts at higher pressures become consistent if melting takes place at 'fluid-absent' conditions or if high melt fractions (and thus low H_2O contents in the melt) are reached.

GPa in the present study, is incompatible with the presence of phengites beyond the dissolution temperature in experiments supposed to have higher bulk H_2O contents and H_2O/K_2O ratios [7,12,13]. However, such phengites may persist if there were fluid losses during the experiment. In other words, experiments carried out under 'fluid-absent' conditions might retain phengite. In such cases, phengite may have reached its maximum temperature stability. Three experiments would have to be reinterpreted this way (Fig. 11).

The three experiments of Irifune et al. [13] and Ono [7] in which a melt quenched to a glass was identified could be interpreted in terms of a "fluid-absent" melting reaction. In Fig. 11, we tentatively located a solidus causing the first occurrence of a supercritical melt through the discontinuous reaction

phengite + clinopyroxene + coesite
= supercritical melt ± garnet.

This melting reaction would have been termed "fluid-absent" at lower pressures, but such a characterization becomes incorrect at conditions above the critical curve. In our interpretation, such melting of phengite at pressures above 5 GPa would result in relatively large melt fractions, melts would then have low H_2O-contents, become quenchable, and observable as silicate glasses in experiments. In fact, the melt compositions at 6 GPa measured by [7] are very similar to our compositions at 4–5 GPa.

In summary, for metapelitic compositions, we propose a termination of the wet solidus not far above 5 GPa, a dissolution of phengite under "fluid-saturated" conditions between 1000 and 1100 °C (at moderate bulk H_2O-contents of a few wt.%), and, at "fluid-absent conditions", i.e. for bulk compositions between phengite and anhydrous phases, "fluid-absent" melting of phengite at 1200 to 1350 °C at 6 to 9 GPa, respectively. The phengite to K-hollandite transition is situated around 9 GPa (and thus, about 1 GPa lower in metasediments than in metabasalts, see Fig. 3).

6. Transport of potassium beyond 300 km depth vs. transfer to and metasomatism of the mantle wedge

Our study shows that in subduction zones phengite is the key mineral for the generation of a mobile phase at depths greater than 100 km. This has geochemical implications as many key tracers for subducted crust

are concentrated in phengite (B, Rb, Ba, and Be) [21]. Loss of phengite leaves an almost potassium free, essentially dry oceanic crust, and although some hydrogen can be stored in nominally anhydrous minerals [38], such a crust is refractory even at the hottest subduction zone conditions [39]. As the potassic phase dissolves in a supercritical melt even at relatively low H_2O-contents, the loss of phengite is extremely sensitive to the actual water/rock ratios in the subducted lithosphere.

The determination of melting temperatures for MORB and sediments to 5 GPa provides an integrated melting scenario for stratified subducting oceanic crust (i.e., an uppermost layer of sediments, hydrated MORB, and moderately hydrated gabbro underlain by partly serpentinized peridotite). When considering thermal gradients in subducting crust, the minimum temperature required for fluid-saturated sediment melting (850 °C at 4 GPa) implies that the underlying MORB must reach temperatures above lawsonite stability (710 °C [4]), as the bottom of a 3-km-thick MORB layer will be less then 100 °C cooler than the sediments [40]. At the same time, the peridotite underlying the mafic crust will be at temperatures 150–250 °C lower than the sediments, which is close to the limit of serpentine stability (660 °C at 4 GPa [41]). With such thermal conditions, fluid production within the MORB would terminate with zoisite breakdown around 3 GPa. Watson and Lupulescu [42] showed that fluid-connectivity in a clinopyroxenite is established somewhere between 1.2 and 2.4 wt.% (aqueous) fluid, and a static eclogite may retain such an amount of fluid from previous dehydration. To what extent this "internal" fluid source remains stable in the potentially strained environment at the slab/mantle wedge interface is unknown at present. Other fluid-sources at >3 GPa are: (i) the gabbroic layer of the oceanic crust, which, at somewhat cooler temperatures than the MORB layer, remains in the lawsonite±chloritoid stability field to higher pressures and at >3 GPa may provide about 0.2–0.4% H_2O relative to his own mass [43], and (ii) the uppermost serpentinized peridotite of the subducting plate. If temperatures in this latter layer overstep serpentine stability, a pulse of aqueous fluid would be produced over a relatively narrow depth range and promote sediment melting through flushing at high pressures.

It should be pointed out, that the above scenario is valid for a stratified oceanic crust typically produced at fast spreading ridges (53% of present day oceanic crust subduction, mainly in the Pacific [44]) but that oceanic crust from slow spreading or in marginal basins has none or much less stratification and thus much less-systematic temperature differences between its different lithological units. As pointed out by Kelemen et al. [45] this picture might be further complicated by mass transfer across the Benioff zone [45,46].

Initial melt compositions from phengite-dominated melting are highly siliceous potassic granites. Thus, Na-rich layers in high-pressure eclogites cannot represent high-pressure melts at low melt fractions, contrary to a previous suggestion [47]. Instead, the refractory residue will be slightly Na-enriched. Thus, anomalously high Na/K ratios could be an indication of previous extraction of high-pressure melts. In case of migration of these high-pressure melts into the overlying mantle wedge, the resulting metasomatism will be similar to that caused by the potassic supercritical melt originating from higher pressures. The Finero peridotite (Ivrea Zone, Southern Alps), in which K_2O-addition occurred with no evidence for bulk Na_2O-addition [48], has probably been metasomatised by such an agent. We suggest that potassium anomalies in the mantle, which are an essential prerequisite for the production of ultrapotassic magmas such as lamproites or kamafugites [49], are generated either by high-pressure melts or by supercritical melt solutions originating from the oceanic crust as identified in this study.

7. Concluding remarks

Our experiments imply that carbonate-free lithologies of the subducting crust are composed of an eclogitic phengite+clinopyroxene+garnet±coesite/stishovite±kyanite±rutile assemblage at near-solidus temperatures and depths between 100 and 300 km. Different bulk compositions will be expressed mostly by different modal proportions, jadeite contents in clinopyroxene, X_{Mg} values, and amounts of *tschermak*-exchange in garnet, clinopyroxene, and phengite.

Between 5 and 6.5 GPa, petrogenetic processes change from classical discontinuous fluid-present melting to continuous dissolution. Discrepancies in

previous experiments can be consistently reinterpreted when the critical endpoint of the fluid-saturated solidus is taken into account and when the contrasting effects of the closure of the solvus between fluid and melt on fluid-present and fluid-absent reactions are considered. In geochemistry, solubilities of trace elements (e.g., U vs. Th) in the mobile phase are used to ascribe metasomatism of the mantle wedge to fluid or melt. However, when H_2O-contents decrease in fluids and increase in melts with increasing pressure, solution properties and thus partition coefficients of the two phases will converge [45]. Distinction between trace element patterns characteristic for fluid or melt may become difficult well below pressures of the critical endpoint and any interpretation of fluxes below arcs in terms of fluid- or melt-transport will have to be reevaluated when trace-element solubilities in supercritical melts become available.

References

[1] J.E. Ricci, The Phase Rule and Heterogeneous Equilibrium, Dover Publications, New York, 1951, 505 pp.

[2] I. Kushiro, A petrological model of the mantle wedge and lower crust in the Japanese island arcs, in: B.O. Mysen (Ed.), Magmatic Processes: Physicochemical Principals, Spec. Publ.-Geochem Soc., vol. 1, 1987, pp. 165–181.

[3] P.J. Wyllie, Magma genesis, plate tectonics, and chemical differentiation of the Earth, Rev. Geophys. 26 (1988) 370–404.

[4] M.W. Schmidt, S. Poli, Experimentally based water budgets for dehydrating slabs and consequences for arc magma generation, Earth Planet. Sci. Lett. 163 (1998) 361–379.

[5] A.B. Thompson, Dehydration melting of crustal rocks, Rend. Soc. Ital. Mineral. Petrol. 43 (1988) 41–60.

[6] D. Vielzeuf, M.W. Schmidt, Melting relations in hydrous systems revisited: application to metapelites, metagreywackes and metabasalts, Contrib. Mineral. Petrol. 141 (2001) 251–267.

[7] S. Ono, Stability limits of hydrous minerals in sediment and mid-ocean ridge basalt compositions: implications for water transport in subduction zones, J. Geophys. Res. 103 (1998) 18253–18267.

[8] P. Ulmer, V. Trommsdorff, Phase relations of hydrous mantle subducting to 300 km, in: Y.W. Fei, C. Bertka, B.O. Mysen (Eds.), Mantle Petrology: Field Observations and High Pressure Experimentation: A Tribute to Francis R. (Joe) Boyd, Spec. Publication-Geochemical Society, vol. 6, 1999, pp. 259–281.

[9] D.J. Frost, The stability of dense hydrous magnesium silicates in earth's transition zone and lower mantle, in: Y. Fei, C.M. Bertka, B.O. Mysen (Eds.), Mantle Petrology: Field Observations and High pressure Experimentation: A Tribute to F.R. Boyd, Spec. Publ.-Geochem. Soc., vol. 6, 1999, pp. 283–296.

[10] J.F. Molina, S. Poli, Carbonate stability and fluid composition in subducted oceanic crust: an experimental study on H_2O–CO_2 bearing basalts, Earth Planet. Sci. Lett. 176 (2000) 295–310.

[11] G.M. Yaxley, G.P. Brey, Phase relations of carbonate-bearing eclogite assemblages from 2.5 to 5.5 GPa: implications for petrogenesis of carbonatites, Contrib. Mineral. Petrol. 146 (2004) 606–619.

[12] K.J. Domanik, J.R. Holloway, The stability and composition of phengitic muscovite and associated phases from 5.5 to 11 GPa: implications for deeply subducted sediments, Geochim. Cosmochim. Acta 60 (1996) 4133–4150.

[13] T. Irifune, A.E. Ringwood, W.O. Hibberson, Subduction of continental crust and terrigenous and pelagic sediments: an experimental study, Earth Planet. Sci. Lett. 126 (1994) 351–368.

[14] M.C. Johnson, T. Plank, Dehydration and melting experiments constrain the fate of subducted sediments, Geochem. Geophys. Geosyst. 1 (1999) Paper 1999GC000014.

[15] D. Vielzeuf, J.R. Holloway, Experimental determination of the fluid-absent melting relations in the pelitic system: consequences for crustal differentiation, Contrib. Mineral. Petrol. 98 (1988) 257–276.

[16] A.E. Patino Douce, J.S. Beard, Dehydration-melting of biotite gneiss and quartz amphibolite from 3 to 15 kbar, J. Petrol. 36 (1995) 707–738.

[17] K.T. Winther, R.C. Newton, Experimental melting of hydrous low-K tholeiite: evidence on the origin of Archean cratons, Bull. Geol. Soc. Den. 39 (1991) 213–228.

[18] E. Auzanneau, D. Vielzeuf, M.W. Schmidt, Biotite stability conditions and the formation of eclogitic assemblages in subducted continental crust: an experimental approach, J. Conf. Abstr. 6 (2001) 346.

[19] M.W. Schmidt, Experimental constraints on recycling of potassium from subducted oceanic crust, Science 272 (1996) 1927–1930.

[20] D.M. Kerrick, J.A.D. Connolly, Metamorphic devolatilization of subducted marine sediments and transport of volatiles to the earth's mantle, Nature (2001) 293–296.

[21] K.J. Domanik, R.L. Hervig, S.M. Peacock, Beryllium and boron in subduction zone minerals: an ion microprobe study, Geochim. Cosmochim. Acta 57 (1993) 4997–5010.

[22] A.L. Boettcher, P.J. Wyllie, The system CaO–SiO_2–CO_2–H_2O—III. Second critical end-point on the melting curve, Geochim. Cosmochim. Acta 33 (1969) 611–632.

[23] H. Bureau, H. Keppler, Complete miscibility between silicate melts and hydrous fluids in the upper mantle: experimental evidence and geochemical implications, Earth Planet. Sci. Lett. 165 (1999) 187–196.

[24] R. Stalder, P. Ulmer, A.B. Thompson, D. Günther, High pressure fluids in the system MgO–SiO_2–H_2O under upper mantle conditions, Contrib. Mineral. Petrol. 140 (2001) 607–618.

[25] G.C. Kennedy, G.J. Wasserburg, H.C. Heard, R.C. Newton, The upper three-phase region in the system SiO_2–H_2O, Am. J. Sci. 260 (1962) 501–521.
[26] S.R. Bohlen, A.L. Boettcher, The quartz–coesite transformation: a precise determination and the effects of other components, J. Geophys. Res. 87 (1982) 7073–7078.
[27] J. Susaki, M. Akaogi, S. Akimoto, O. Shimura, Garnet–perovskite transformation in $CaGeO_3$: in-situ X-ray measurements using synchrotron radiation, Geophys. Res. Lett. 12 (1985) 729–732.
[28] J. Zhang, B. Li, W. Utsumi, R.C. Liebermann, In-situ X-ray observation of the coesite–stishovite transition: reversed phase boundary and kinetics, Phys. Chem. Miner. 23 (1996) 1–10.
[29] D. Vielzeuf, J.M. Montel, Partial melting of Al–metagreywackes: Part I. Fluid absent experiments and phase relationships, Contrib. Mineral. Petrol. 117 (1994) 375–393.
[30] R.G. Cawthorn, K.D. Collerson, The recalculation of pyroxene end-member parameters and the estimation of ferrous and ferric iron content from electron microprobe analyses, Am. Mineral. 59 (1974) 1203–1208.
[31] W.L. Huang, P.J. Wyllie, Phase relationships of *S*-type granite with H_2O to 35 kbar: muscovite granite from Harney Peak, South Dakota, J. Geophys. Res. 86 (1973) 10515–10529.
[32] G.T. Nichols, P.J. Wyllie, Ch.R. Stern, Subduction zone melting of pelagic sediments constrained by melting experiments, Nature 371 (1994) 785–788.
[33] D. Ryabchikov, Ch. Miller, P.W. Mirwald, Composition of hydrous melts in equilibrium with quartz eclogites, Mineral. Petrol. 58 (1996) 101–110.
[34] J. Hermann, Experimental constraints on phase relations in subduction continental crust, Contrib. Mineral. Petrol. 143 (2002) 219–235.
[35] G. Hoschek, Melting and subsolidus reactions in the system K_2O–CaO–MgO–Al_2O_3–SiO_2–H_2O: experiments and petrologic application, Contrib. Mineral. Petrol. 105 (1990) 393–402.
[36] O. Paillat, S.C. Elphick, W.L. Brown, The solubility of water in $NaAlSi_3O_8$ melts—A reexamination of Ab-H_2O phase–relationships and critical behaviour at high-pressures, Contrib. Mineral. Petrol. 112 (1992) 490–500.
[37] A.H. Shen, H. Keppler, Direct observation of complete miscibility in the albite–H_2O system, Nature 385 (1997) 710–712.
[38] J. Ingrin, H. Skogby, Hydrogen in nominally anhydrous upper-mantle minerals: concentration levels and implications, Eur. J. Mineral. 12 (2000) 543–570.
[39] K. Hirose, Y. Fei, Y. Ma, H.K. Mao, The fate of subducted basaltic crust in the Earth's lower mantle, Nature 397 (1999) 53–56.
[40] C. Kincaid, I.S. Sacks, Thermal and dynamical evolution of the upper mantle in subduction zones, J. Geophys. Res. 102 (1997) 12295–12315.
[41] P. Ulmer, V. Trommsdorff, Serpentine stability to mantle depths and subducted related magmatism, Science 268 (1995) 858–861.
[42] E.B. Watson, A. Lupulescu, Aqueous fluid connectivity and chemical transport in clinopyroxene-rich rocks, Earth Planet. Sci. Lett. 117 (1993) 279–294.
[43] S. Poli, M.W. Schmidt, Petrology of subducted slabs, Annu. Rev. Earth Planet. Sci. 30 (2002) 207–235.
[44] M.W. Schmidt, S. Poli, Generation of mobile components during subduction of oceanic crust, Treatise Geochem. 3 (2003) 567–591 (Elsevier).
[45] P.B. Kelemen, K. Hanghj, A.R. Greene, One view of the geochemistry of subduction-related Magmatic Arcs, with an emphasis on primitive andesite and lower crust, Treatise Geochem. 3 (2003) 593–659.
[46] T.V. Gerya, D.A. Yuen, Rayleigh–Taylor instabilities from hydration and melting propel 'cold plumes' at subduction zones, Earth Planet. Sci. Lett. 212 (2003) 47–62.
[47] W. Schreyer, H.J. Massone, C. Chopin, Continental crust subducted to depths near 100 km: implications for magma and fluid genesis in collision zones, in: B.O. Mysen (Ed.), Magmatic Processes: Physicochemical Principals, Spec. Publ. Geochem. Soc. 1 (1987) 155–163.
[48] A. Zanetti, M. Mazzucchelli, G. Rivalenti, R. Vannucci, The Finero phlogopite–peridotite massif: an example of subduction-related metasomatism, Contrib. Mineral. Petrol. 134 (1999) 107–122.
[49] S. Foley, Petrological characterization of the source components of potassic magmas: geochemical and experimental constraints, Lithos 28 (1992) 187–204.
[50] H. Martin, Adakitic magmas: modern analogues of Archean granitoids, Lithos 46 (1999) 411–429.